NANO · MICRO
small

Supporting Information

for *Small*, DOI 10.1002/smll.202405000

All-Metal Flexible Fiber by Continuously Assembling Nanowires for High Electrical Conductivity

Chengqiang Tang, Kailin Zhang, Sihui Yu, Hang Guan, Mingjie Cao, Kun Zhang, You Pan, Songlin Zhang, Xuemei Sun and Huisheng Peng**

Supporting Information

All-metal flexible fiber by continuously assembling nanowires for high electrical conductivity

Chengqiang Tang†, Kailin Zhang†, Sihui Yu, Hang Guan, Mingjie Cao, Kun Zhang, You Pan, Songlin Zhang, Xuemei Sun, and Huisheng Peng**

C. Tang, K. Zhang, S. Yu, H. Guan, M. Cao, Kun. Zhang, Y. Pan, Prof. S. Zhang, Prof. X. Sun, Prof. H. Peng
State Key Laboratory of Molecular Engineering of Polymers, Department of Macromolecular Science, Institute of Fiber Materials and Devices, and Laboratory of Advanced Materials, Fudan University; Shanghai, 200438, China.
E-mail: sunxm@fudan.edu.cn, penghs@fudan.edu.cn.

†These authors contributed equally to this work.

This file includes:
Figure S1 to S13 (Pages S2-S14)
Caption for Supplementary Movie (Page S15)

Figure S1. Photograph of the AFE wrapped around a glass tube.

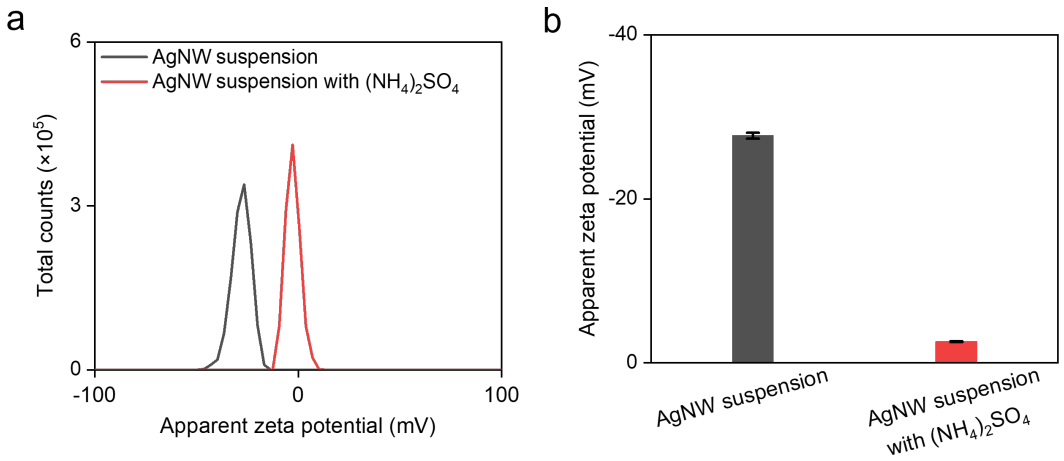

Figure S2. (a) Zeta potential intensity distributions and (b) average values for PVP cladded AgNW suspension and AgNW suspension with $(NH_4)_2SO_4$. N=3. Data are shown as mean ± SD.

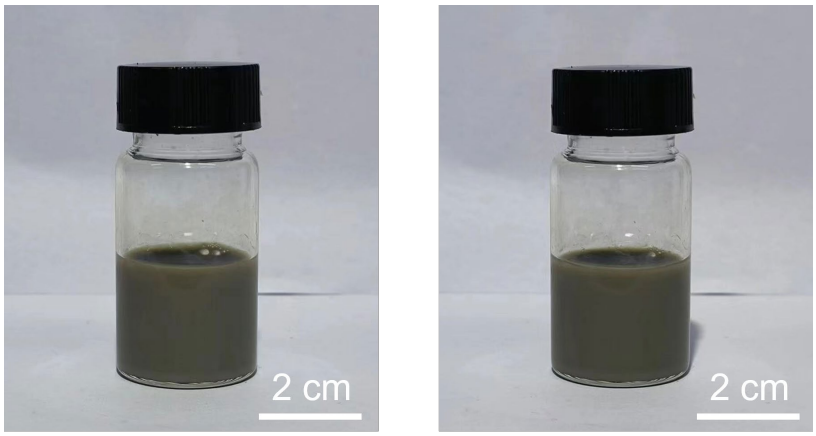

Figure S3. Photographs showing the stable spinning solution at different time points.

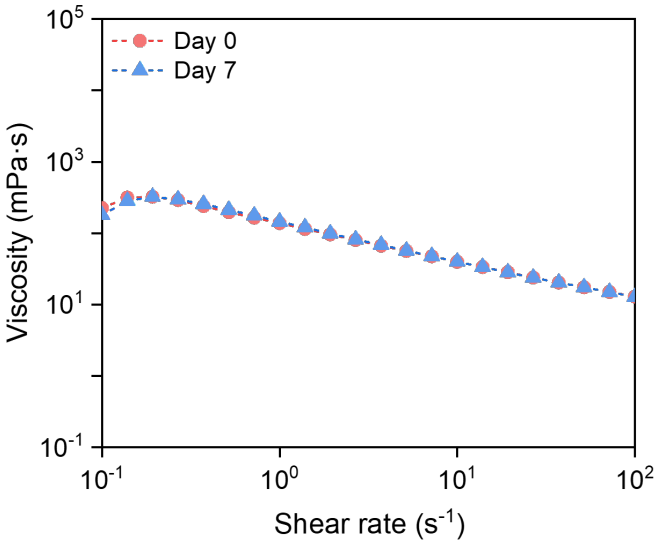

Figure S4. Apparent viscosity as a function of shear rate for the spinning solution at different time points.

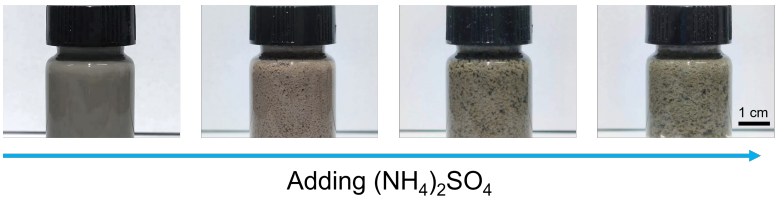

Figure S5. Photographs showing the changes in the AgNW suspension after the continuous addition of $(NH_4)_2SO_4$. From left to right, the concentrations of $(NH_4)_2SO_4$ are 0, 200, 500, and 700 $mg \cdot mL^{-1}$.

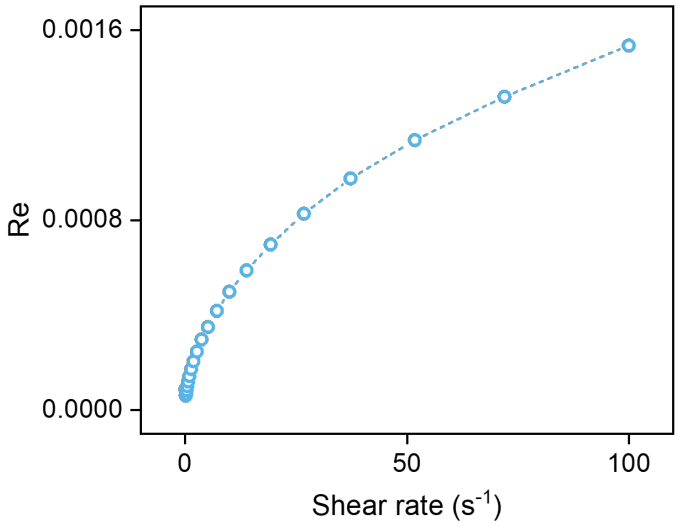

Figure S6. Reynolds number (Re) as a function of shear rate for the spinning solution.

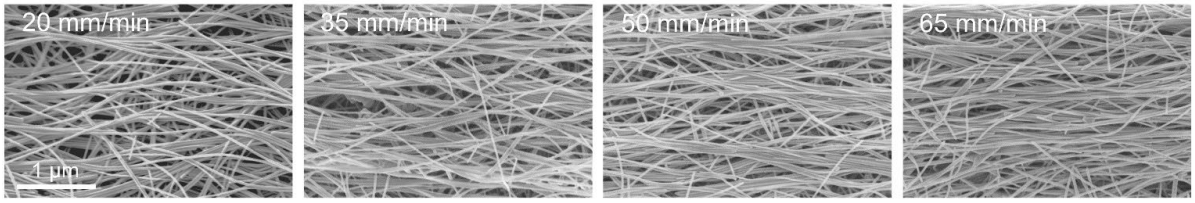

Figure S7. FESEM images of AFEs obtained at increasing extruding speeds.

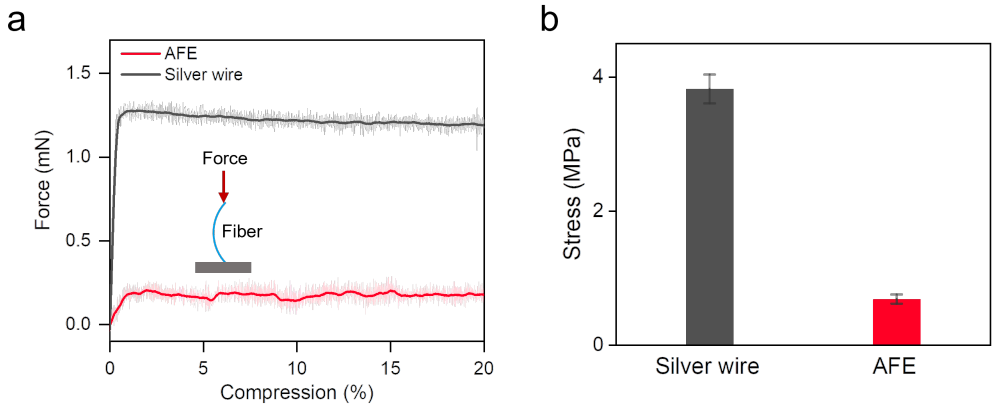

Figure S8. (a) Bending forces and (b) calculated maximum bending stresses of the AFE and the silver wire with the same dimension. N=3. Data are shown as mean ± SD.

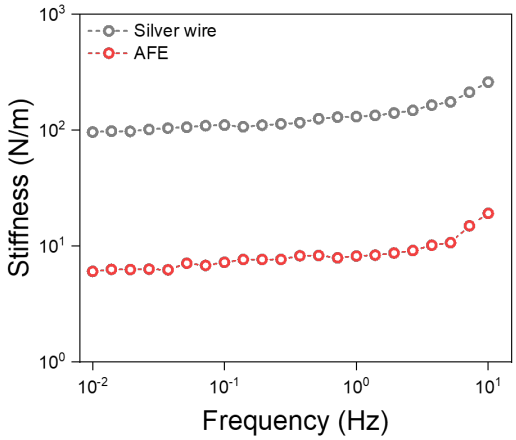

Figure S9. The bending stiffnesses of the AFE and silver wire. Bending stiffness was tested at a frequency sweep of 0.01–10 Hz (covering frequency range of the human respiration and heartbeat) under controlled displacement (50 μm) at 25 °C using a dynamic mechanical analyzer (Q850, TA Instruments). The AFE and silver wire had the same dimension.

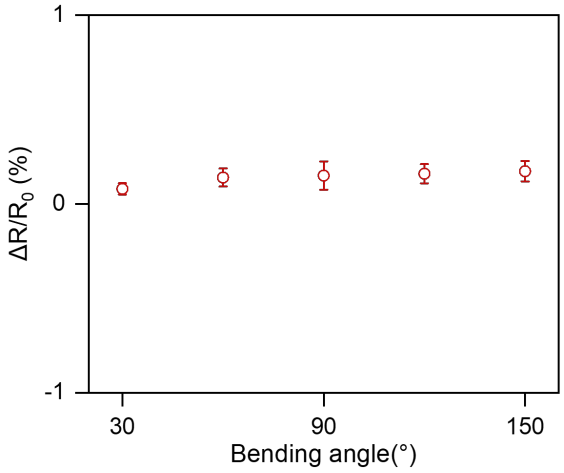

Figure S10. Resistance changes of AFEs under bending at different angles (N=3). Data are shown as mean ± SD. Samples with the length of 5 cm were used.

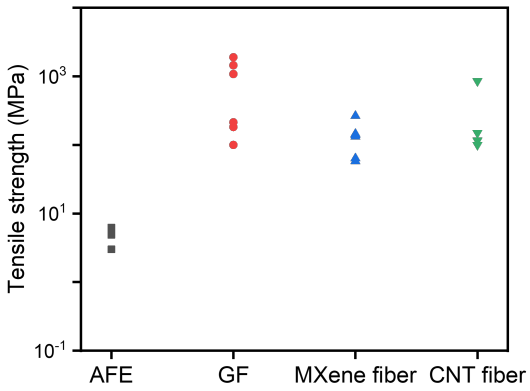

Figure S11. Tensile strength comparison of AFEs with other nanomaterial-based fiber electrodes.

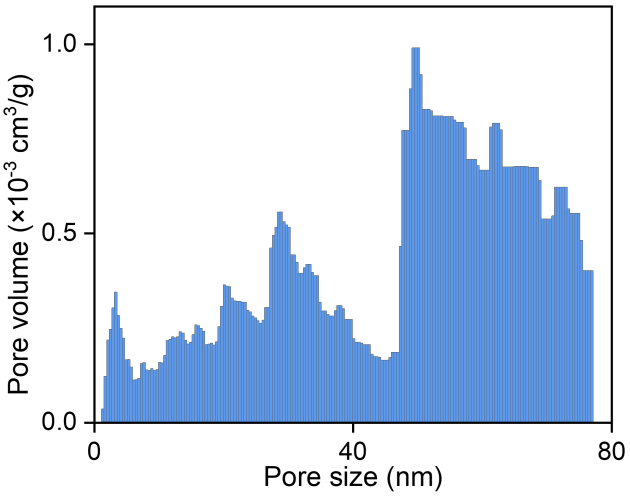

Figure S12. Pore size distribution of the AFE based on DFT model N_2 adsorption isotherms.

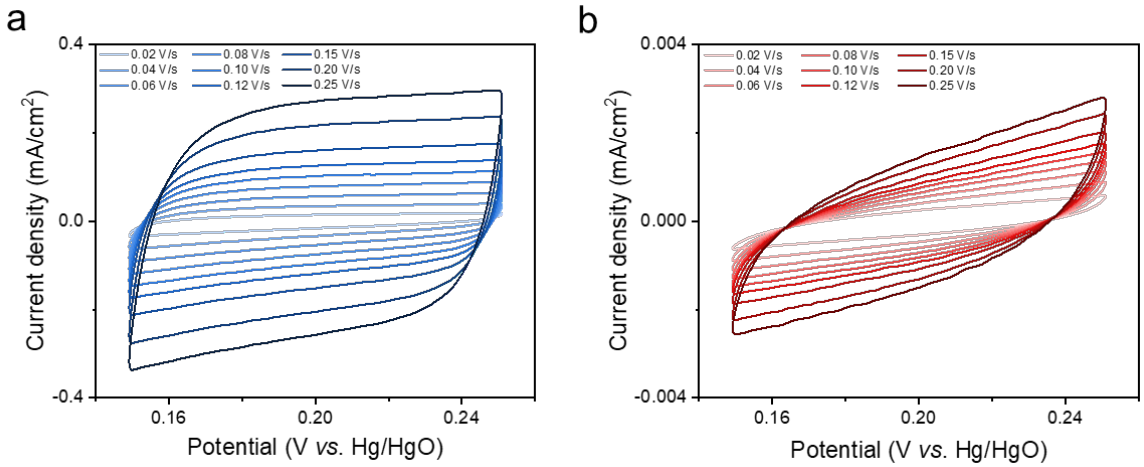

Figure S13. Cyclic voltammetry curves of (a) AFE and (b) bulk Ag wire in 0.1 M KF electrolyte at different scan rates.

Caption for Supplementary Movie

Movie S1 | Stable extruding of AgNWs spinning solution during continuous fabrication of all-metal fiber electrode.